Sensors & Actuators: A. Physical 383 (2025) 116187

Contents lists available at ScienceDirect

Sensors and Actuators: A. Physical

journal homepage: www.journals.elsevier.com/sensors-and-actuators-a-physical

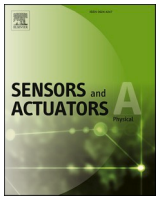

Ion-wind powered boat using a novel wire-dielectric water system

Ngoc Luan Mai [a,*], Tuan-Khoa Nguyen [b], Canh-Dung Tran [c], Trung-Hieu Vu [a], Thien Xuan Dinh [d], Nam-Trung Nguyen [b], Dzung Viet Dao [a,b], Van Thanh Dau [a,*]

[a] School of Engineering and Built Environment, Griffith University, Queensland 4215, Australia
[b] Queensland Micro and Nano Technology Centre, Griffith University, Queensland 4111, Australia
[c] School of Mechanical and Electrical Engineering, University of Southern Queensland, Queensland 4350, Australia
[d] The Commonwealth Scientific and Industrial Research Organization, Australia

ARTICLE INFO

Keywords:
Corona discharge
Electrohydrodynamic propulsion
Ion wind
Thrust-to-power

ABSTRACT

In the era of tightening environmental regulations and fast rising fossil fuel costs, green-energy propelling technologies have been in great demand for the maritime industry. By the electrohydrodynamic propulsion, this work demonstrates the launch of an ion-wind powered boat (*i*Boat) that offers a novel propeller-free approach with insignificant noise and rather low power consumption. The innovative design of the *i*Boat includes a conducting wire functioning as the emitter, while the water surface was exploited as the downstream electrode, thus, eliminating the need for the second electrode which is typically essential for the ion wind generation. The proposed ion wind propulsion system can generate a thrust-to-power ratio of 1.45 mN/W using a simple wire-dielectric-water configuration. In the experiment, we successfully launch the *i*Boat carrying payloads of 120 g with wiring connected to the external power supply system. This novel concept can potentially pave the way for the future development of propeller-free boats with insignificant noise in real-life applications including army and wildlife surveillance missions.

1. Introduction

The electrohydrodynamic (EHD) systems have attracted a great deal of interest in research and developments since the pioneering discovery of Chattock [1] on a flow of ionized air generated by the corona discharge created by a strong electric field, known as the electron avalanche phenomenon. Generally, the Coulomb force causes the ionized molecules of air to collide with and transfer their momentum to neutral ones to generate ionic winds of significant thrust power. The Coulomb force by the interaction among charged molecules, named volumetric electrohydrodynamic for propulsion of a "silent and simple ion engine power" was actively progressed since Robinson's work [2] in which he stated a conversion efficiency of around only 1 %. This was confirmed by Goldman et al. [3] and also in several other publications using various electrode arrangements, such as point-to-plane [4], point-to-grid [5], point-to-ring [6], or wire-to-plate [7], multipin-to-ring [8]. This conversion efficiency was reported to reach 1.72 % in an optimized point-to-grid configuration [9].

Corona discharge and its accompanied ion wind are usually utilized in many important applications including heat transfer enhancements [10], nano assisted coating/deposition [11], electrostatic generator [12], and propulsion systems [13], drying and enhanced combustion applications [14]. The advantages of this approach in generating ion wind include fast response, low energy consumption, simple and compact structure (no moving parts) compared with conventional methods. Furthermore, optimized large-size ionic wind, known as external propulsion, showed a great velocity promotion [15] and fast response load control [16]. Besides the traditional EHD systems, several modified configurations, for example wire-to-inclined wing [17], point-to-wire [18], parallel plates [19], needle-to-needle [20], point-to-parallel plate [21], wire-to-cylinder [22–24], sphere-to-sphere [25], point-to-cylinder [26], and oppositely charged dual-pin [27–29] were recently reported.

Over the last three decades, a great deal of effort has been devoted in developing the ion-wind based propulsion. In such works, thrust is introduced into the electric input power ratio (θ) and the airflow area ratio (Φ) as the essential parameters to investigate and evaluate the system efficiency [30]. For example, several publications found that with an optimization of θ and Φ up to 20 N/kW and 20 N/m^2, respectively at the atmospheric pressure as well as the sea level, ion winds can

* Corresponding authors.
E-mail addresses: luan.mai@griffithuni.edu.au (N.L. Mai), v.dau@griffith.edu.au (V.T. Dau).

https://doi.org/10.1016/j.sna.2024.116187
Received 6 August 2024; Received in revised form 12 November 2024; Accepted 27 December 2024
Available online 28 December 2024

generate a sufficiently strong propulsion in aerospace applications [31, 32]. Although such an optimization is challenging, several techniques including multiple stages and alternating positive/negative discharge were proposed to generate significantly strong propulsions [33]. Recently, a toroidal counter electrode for ionic propulsion has been proposed [34], which can yield upto 288.55 mN of thrust and 23.15 N/m^2 of airflow area ratio. This setup utilizes ionic wind to rotate propeller, thus may creating noise and vibration as in conventional turboprop apparatus.

The EHD based propulsion perspective was recently demonstrated by the first take-off of ionic wind based flying device [13] and a gliding flight of EHD powered aero-plane [35]. The unprecedented flights showed the potential of ion wind technique in generating a thrust density of about 7 N/m^2 or a thrust of 5 N/kW by optimizing the aerodynamic design of miniaturized aircraft. Since the devices are in-atmosphere both electrodes of EHD are installed on their body; and conventional flaps are used to control the direction of the EHD ion wind. Additionally, to optimize the weight of EHD power supply system for heavier-than-air aircrafts, a wireless power transmission system has been developed and proven feasible for in-atmosphere ionocrafts [36].

The recent enhancement of EHD used propulsion allows to develop unprecedented platform for maritime applications without the use of propeller-based engine which is not environmentally friendly (making noise) and especially not ideal for military applications. Aligning with this approach, this work has developed the first launch of ion-wind powered boat (named as *i*Boat) operated by EHD based propulsion using our novel wire-dielectric-water configuration. The EHD based new structure takes advantage of water surface as the system's downstream electrode, playing the role of a collector, meanwhile a dielectric plate (also called flap) of polypropylene is installed to navigate the direction of electric field. That controls the thrust in both direction and magnitude, thus controlling the boat's motion. In other words, the novel configuration does not use any ground electrode attached to the device but introduces a dielectric as a flap for both electric and aerodynamic fields to direct the EHD ion wind. As an illustration of the new concept, the first miniaturized *i*Boat powered by the ion wind thrust is successfully sailed, featuring simple configuration, quiet moving and small power consumption for a range of supplied voltages from 3 kV to 18 kV. An achieved thrust-to-power ratio of 1.45 mN/W is able to drive the *i*Boat carrying a load of 120 g, without considering the weight of the power supply system. This initial performance demonstrates the feasibility and of the present EHD system yet indicates the need for future development and optimization.

2. New concept of iboat & mechanism

A typical configuration of ion wind generation system consists of a sharply curved electrode (pin or small diameter wire) which plays the role of an emitter and a less curved counter-electrode (most commonly a plane) as a collector [16]. By a sufficiently high electric field, a cylindrical region with a diameter of $\sqrt{D}$ surrounding of the emitter is ionized, where D (mm) is the diameter of the emitter. The momentum of the ionized particles is transferred to the neutral particles through their impacts, thus generating the thrust.

The present *i*Boat includes a circular wire of 0.1 mm in diameter, acting as the emitter which is installed parallel to the water surface at a distance d at the boat stern (see Fig. 1A). By an applied relevant voltage, a strongly concentrated electric field ionizes air molecules and includes corona discharge due to electron avalanche in ionized region. This ionization zone is composed of electrons and ions. Positive ions are predominantly produced in the case of high positive voltage, and negative ions are primarily produced in the case of high negative voltage. Every ion is subjected to Coulomb forces and is displaced out of the ionization zone into the drift region. In this region, the ions do not have sufficient energy for further charge creation owing to the low electric field. Here, the ions collide with neutral air molecules and transfer momentum with each collision [37]. This process drifts the air and generates ion wind toward the water surface, which plays the role of the ground electrode (Fig. 1B).

It is worth noting that for this approach, since the water surface acts as the collector, it is not necessary to install a second electrode downstream as requested in the previous works. Therefore, in our new EHD system, ion winds are successively generated from the wire (emitter) to the water surface. The mechanism of the present system as illustrated in Fig. 1 can be described as follows. An ion wind generated perpendicular to the water surface creates a force in the tangential direction with the ion wind flow, which is transformed into an optimized horizontal force by a dielectric flap (see Fig. 1A). This flap is installed between the wire and water to adjust the electric field generated by electrodes (the wire and the water surface). As a result, at an optimal position of the flap, the generated force is converted into a sufficiently strong thrust that propels the *i*Boat forwarding. Our experimental results shown the parameters including the distance between the wire and water surface (d) and the inclination of dielectric flap (angle δ) can be optimized to reach a desired thrust.

3. Numerical simulation and results

In order to highlight the physical properties of the new concept based EHD model (Fig. 1A), the 2-D multi-physic simulation of *i*Boat is carried out using the conservation equations of mass and momentum (for air flow field) coupled with the equations of Poisson and charge conservation (for electric and charge field) [38–40].

For electric and charge field, neglecting the conduction and diffusion of ions in the atmosphere, the movement of a charge q generated at the emitter (wire electrode) is governed by the equation of the charge

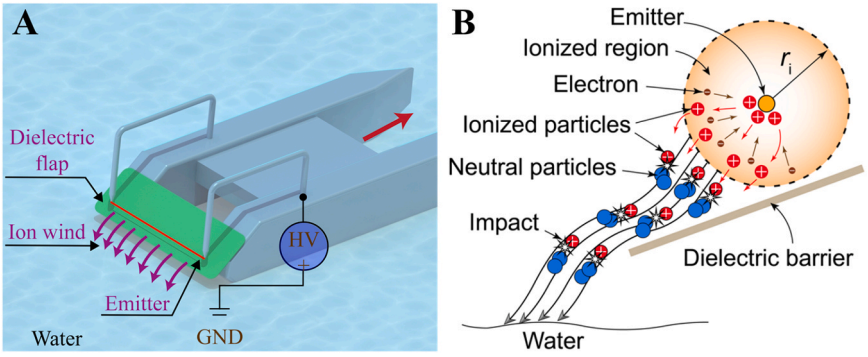

Fig. 1. Mechanism of ion wind powered boat. **A)** A schema of the present iBoat using a wire (flap) as the emitter and water surface as the collector, and **B)** Working principle of the present iBoat (cross-section view) with the emitter (wire) connected to a high voltage (HV+), creating an ionized cylindrical zone surrounding the wire. Thrust generated by ion wind flows from the wire to the water surface, whose direction is adjusted by a dielectric flap to propel the boat forwards.

conservation and the Gauss' law, respectively as follows,

$$\nabla\cdot(\mu_e \boldsymbol{E}q + \boldsymbol{U}q) = 0, \tag{1}$$

$$\nabla\cdot(\nabla V) = -\frac{q}{\varepsilon}, \tag{2}$$

where $\mu_e = 1.6 \times 10^{-4}$ m^2/(Vs) is the mobility of ions [24]; $\boldsymbol{U}$ the velocity of air drifted by the motion of charge; ε the permittivity of air; and $\boldsymbol{E}$ is the electric field and determined as the gradient of the electric potential $\boldsymbol{E} = -\nabla V$.

Boundary condition on the emitter is set up as the density q_s, which is a function of discharge current (I):

$$q_s = \frac{I}{\mu_e E_{on} A}, \tag{3}$$

where A is the area of the electrodes' surface, I and V are approximated by experiment as depicted in Fig. 5, and $E_{on} = 3.23 \times 10^6$ V/m the onset electric field [41]. The interaction force between charged ions and neutral molecules, consisting of the Coulombic force generated by the electrical charge and permittivity gradient, and the electrostriction force, is defined as the body force and given by

$$\boldsymbol{f}_e = q\boldsymbol{E} - \frac{1}{2}|\boldsymbol{E}|^2\nabla\varepsilon + \frac{1}{2}\nabla\left(|\boldsymbol{E}|^2\rho\frac{\partial\varepsilon}{\partial\rho}\right). \tag{4}$$

Meanwhile for the air flow, assuming *i*Boat works in the environment of air with limited temperature gradient, the last two components of body force in Eq. (4) are neglected. Thus, air flow is steady state and governed by the Navier–Stokes and continuity equations as follow,

$$\nabla\cdot(\boldsymbol{U}\boldsymbol{U}) - \nabla\cdot(\nu\nabla\boldsymbol{U}) = -\nabla p + \frac{q\boldsymbol{E}}{\rho}, \tag{5}$$

$$\nabla\cdot\boldsymbol{U} = 0, \tag{6}$$

where p is the air pressure; $\nu = 15.7 \times 10^{-5}$ m^2/s the kinematic viscosity and $\rho = 1.204$ kg/m^3 the air density.

Thrust (T) by ion wind which is generated by applying a high voltage to the positive electrode (wire) and the ground electrode (water surface), is estimated by the Coulombic force exerting on ions existing between the electrodes [42]

$$T = \int_{\mathrm{V}} qEd\ \mathrm{V} = \int_0^d qEAdx, \tag{7}$$

where q is the charge density, $d\bigvee$ the differential volume, d the distance between the electrodes, A the characteristic area, and E the electric field intensity.

With the discharge current $I = qv_iA$ and the average velocity of ions $v_i = \mu_e E$, introducing these relationships into Eq. (7) yields the thrust as a function of current as

$$T = \frac{Id}{\mu_e}. \tag{8}$$

In this simulation, the 2-D multi-physic transient problem is solved in a considered domain of two different regions for air and flap. Firstly, the problem is time discretized and then at each time step Eqs. (1)-(2) and Eqs. (5)-(6) together with boundary conditions by Eqs. (3)-(4) are solved in the air region for the electrostatic coupled air dynamic system, whilst only Eq. (2) is solved within the flap region, neglecting the polarization effect of a dielectric placed inside an electric field.

It is worth noting that the interface between the two regions is a two-way coupling boundary condition: the electric potential and the impenetrable wall are for electric charge, and no-slip wall for the remaining parameters. Moreover, on the circular emitter' surface, the positive potential and corona conditions are set up using Eq. (3). The geometrical dimensions and meshing topology of the *i*Boat model for simulation are illustrated in Fig. 2. Also, a thin layer which is introduced on the flap boundary (see Fig. 2B) is essential for the generation of surficial charge, which results in the deflection of electric field at the emitter as well as the unbalance of horizontal force. The mechanism of this physical phenomena will be thoroughly discussed below.

The numerical results in Fig. 3 show the ion wind evolution from the transient simulation of the *i*Boat, that clarifies the influence of the flap on the charge density, velocity and developing direction of ion wind. Fig. 3A shows charge (by contours) is emitted and moved in vertical direction and perpendicular to the water surface, resulting in ion wind in the same direction, as shown in Fig. 3E. Thus, the unbalanced force only occurs in the vertical axis, and therefore only lift is generated. Meanwhile, by introducing a flap, both charge and ion wind velocity field are produced and advance to culminate a state where a thrust is generated due to the electric field deflection (Fig. B, C, D, F, G and H). Fig. 3B & C capture states at initial time steps until elapsed time of 0.4 ms in which charge density appears and gradually expands from the emitter to quickly form a dense layer of ions on the flap's surface (see Fig. 4). During this period, electric field penetrates the dielectric medium and leaves charge to form the dense layer. After an adequately elapsed time, the layer of charge induces a potential (as implied in Eq. (2)) sufficiently strong to counteract the emitter potential, that adjusts the electric field surrounding the emitter to generate thrust pushing *i*Boat. Moreover, the ion wind at these timesteps gradually developed following the movement of charge, which yields vortexes as air is deflected by the solid wall of the dielectric flap, shown in Fig. 3F & G. Eventually, the corona discharge and ion wind field establish their stable state, resulting in an adjusted flow and partially converting lift into thrust (Fig. 3H).

Furthermore, for the generation and development of charges with respect to time into ion wind, which eventually creates thrust as shown in Fig. 4, it is noted that the layer of ions on the flap is requested extremely thin but contains an enormous number of charges. Our numerical results show that the charge density measured within a grid element of the layer is a hundred times higher than one of the adjacent regions. That demonstrates the flap's effect on electric field induced by the electrodes. The simulating results also depict the flap configuration, including shape and geometrical dimensions, distance to wire and inclined angle can be used to control the layer of ions in maximizing thrust. The simulation of *i*Boat will be investigated by experiments using the corresponding data and parameters of the model and hence to demonstrate the physical appropriate of the new concept of *i*Boat.

4. Experiment results and discussions

The experiment with *i*Boat model whose configuration and apparatus are presented in Section 1 of the attached Electronic Supplementary Material (EMS) with a range of inter-electrode distances (d) between the emitter (wire) to water surface from 10 to 20 mm is investigated. However, a range from 13 mm to 16 mm is found to achieve optimal force as shown in Fig. 5. In this circumstance, because the force is in the vertical direction, we refer to it as lift to distinguish with the thrust force in the horizontal direction. Fundamentally, our lift force has similar physical definition with the thrust in Eq. 8, that is the force acted in the reversed direction with the corona discharge.

Some experimental results on flapless configuration in Fig. 5 show that with a given distance d, the lift (force in vertical direction) quasi-linearly increases with the increase of the applied voltage. However, at a certain distance d when the applied voltage exceeds a threshold value, the spark occurs, yielding a critical reduction of the force. This experimental observation is in very good agreement with the theoretical approximation by Eq. (8). For example, a maximum lift of 5.6 mN was observed at the distance of 15 mm by applied voltage of 17 kV. Since the experiment was carried out with a source of limited voltage, the spark was not found for inter-electrode distance be equal and greater than 18 mm.

The relationship of thrust versus the inter-electrode distance (d) and

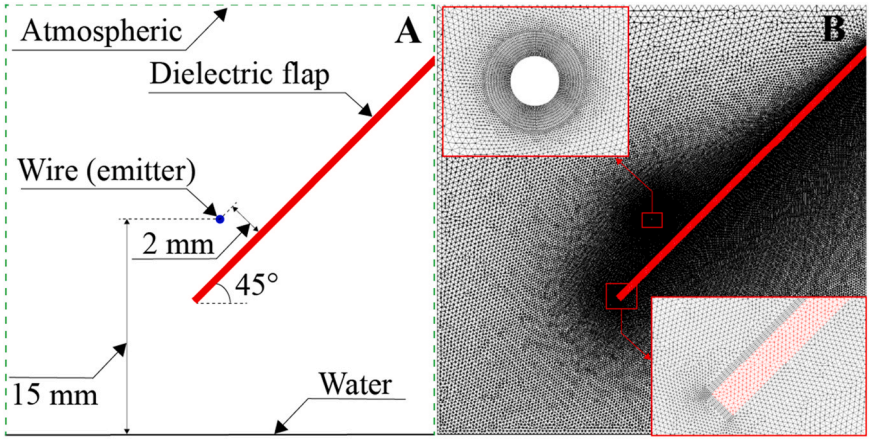

Fig. 2. Numerical simulation of the iBoat. **A)** Geometrical dimensions of considered domain: the emitter (circular wire electrode) is of 0.1 mm in diameter (circumferential area: pi × diameter × length); distance from the emitter to flap is kept at 2 mm in all experiments, and **B)** Meshing topology with note: the emitter and the flap's vicinity are meshed sufficiently fine to capture differential electric field and charge accumulation, respectively, as shown in insets.

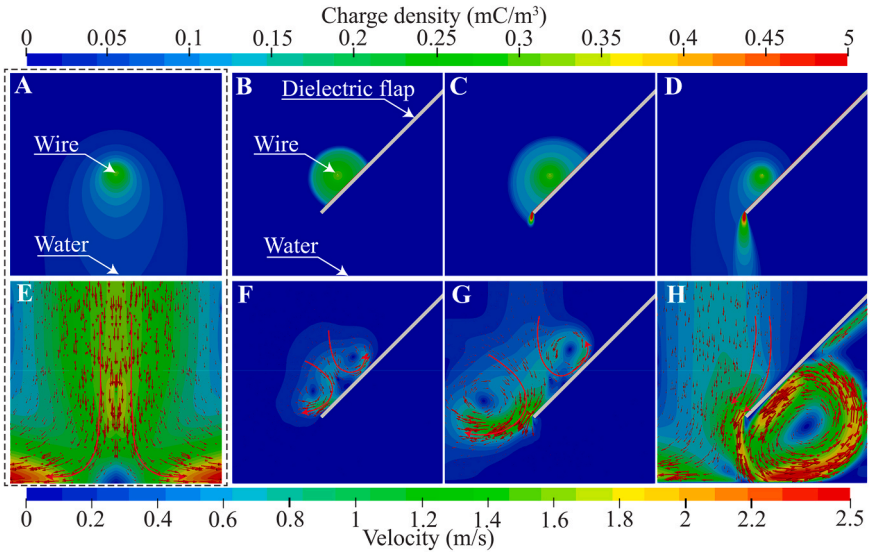

Fig. 3. Simulation results of iBoat. Evolution of the charge density for four cases: **A)** without dielectric flap at elapsed time 5 ms; **B, C, D)** with dielectric flap at elapsed time 0.2 ms, 0.4 ms and 5 ms respectively; contours express **c**harge density in mC/m^3. Evolution of velocity and direction of ion wind for **E)** without dielectric flap at elapsed time 5 ms; **F, G, H)** with dielectric flap at elapsed time 0.2 ms, 0.4 ms and 5 ms respectively; contours and vector field express ion wind velocity and ion wind direction, respectively, red arrows generalize ion wind direction.

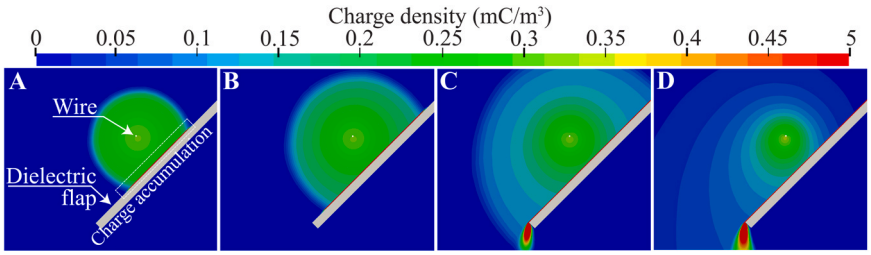

Fig. 4. Simulation results of iBoat. Charge propagation on the upper surface of the flap at several elapsed times: **A)** at 0.1 ms, **B)** 0.2 ms, **C)** 0.4 ms, and **D)** 5 ms. Emitter (wire) and flap are installed as shown in Fig. 2 and contour shows charge density in mC/m^3.

the inclined angle of dielectric plane (δ) is investigated for a range of applied voltages from 3 kV to 18 kV. Experimental results by Fig. 6A show that at an inter-electrode distance (wire – water surface distance), the thrust continuously increases with the increasing of the applied voltage and reaches a maximum when the spark occurs. Furthermore, the maximum thrust increases from $d = 11$ mm and achieves peak at $d = 15$ mm then decreases when d is larger than 15 mm. According to our experimental results, an optimal configuration of *i*Boat with inter-electrode distance of 15 mm was registered to achieve maximum thrust.

In our concept, the equivalent inter-electrode distance compared with the conventional ion wind configuration can be determined from

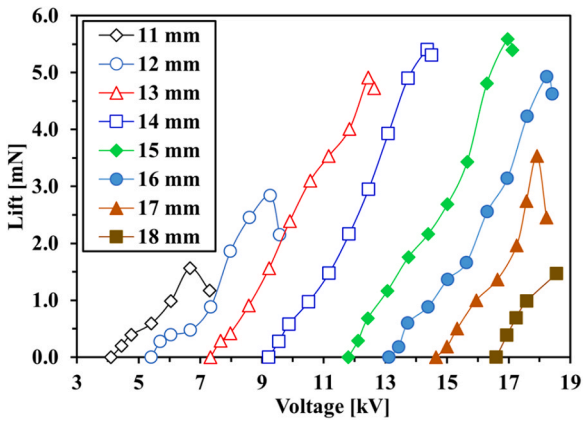

Fig. 5. Experimental results for flapless configuration: Lift generated by ion wind plotted versus applied voltage for a range of electrode distances (wire – water surface) (11, 12, 13, 14, 15, 16, 17 and 18) mm.

Eq. (8) as $\overline{d} = \frac{T\mu_e}{I}$. For instance, the equivalent distance $\overline{d}$ is about 5 mm corresponding to a measured vertical distance of 15 mm. Experimental observation by Fig. 6B also shows that at a given applied voltage, the thrust (T) slightly increases with the increase of the flap's inclined angle (δ) up to 60°. An experimental relationship of thrust T versus the flap's inclined angle δ is proposed as $T = \tau_\delta \frac{Id}{\mu_e}$, where τ_δ is the parameter relating to the inclined angle of the flap. Our experiment found that in general, an optimal thrust is achieved at the flap's inclined angle of 45°.

In addition, our experiment shows that a fully loaded boat (payload and its weight) can achieve a stable velocity $v_d = 0.09$ m/s with an inter-electrode distance d of 15 mm and a $\delta = 45°$ inclined flap angle (see Section 2 in EMS). Considering that the boat's unloaded weight of 15 g (~0.147 N) and a maximum payload 120 g (~1.18 N), a simple calculation by $f_D = \frac{1}{2} C_w \rho_w A_w v_d^2$ (C_w= 1.05 is resistance coefficient of water depending on the Reynolds number, ρ_w (kg/m^3) is the density of water, A_w is the submerged cross-section of the boat varying from 1 cm^2 to 9 cm^2 for unload and fully loaded condition, respectively) yields a corresponding resistance force of around 3.82 mN, which is in reasonably good agreement with the experimental results of thrust in Fig. 6B. This agreement is backed by the fact that at steady boat motion, exerted forces reach an equilibrium $f_D = T$, consolidating the reliability of our model and measurements.

The current-voltage characteristics of ion wind using the present wire-dielectric-water configuration for the boat is established in Fig. 7A with the following relationship [43]

$$I = C(V - V_0)^n, \tag{9}$$

where the exponent n depends on the geometry of the emitter (wire/pin and its diameter), C is a constant related to the material and geometry of the electrode as well as the ion mobility. In this work, the current-voltage characteristics in Fig. 7A is expressed by the relationship $\sqrt{I} \sim V$ where $n = 2$. It is worth noting that this relationship was used to characterize the generation of ion wind in several configurations, for

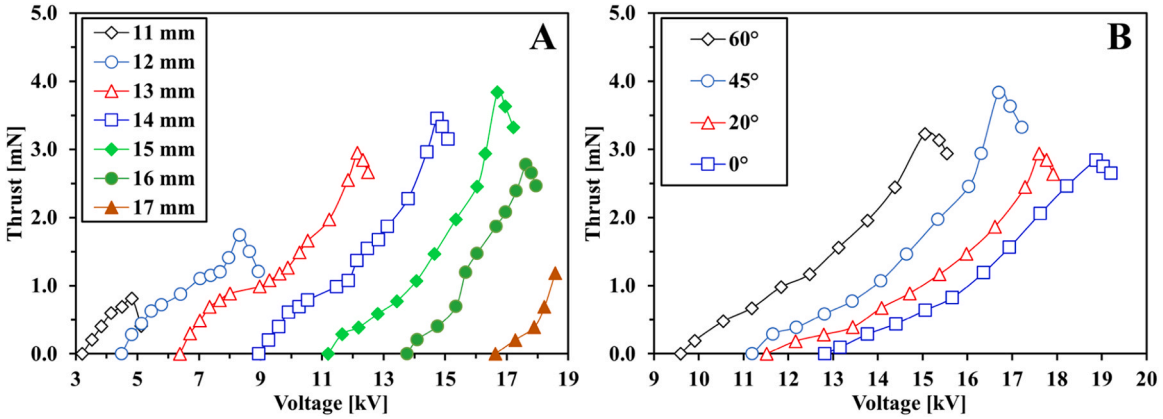

Fig. 6. Experimental results: **A)** Thrust plotted versus applied voltage for a range of wire-water vertical distances [11–17] mm with a flap angle of 45°; and **B)** Thrust plotted versus applied voltage for a range of the flap's inclined angles (δ) (0, 20, 45 and 60)° for an inter-electrode (wire-water) distance d of 15 mm.

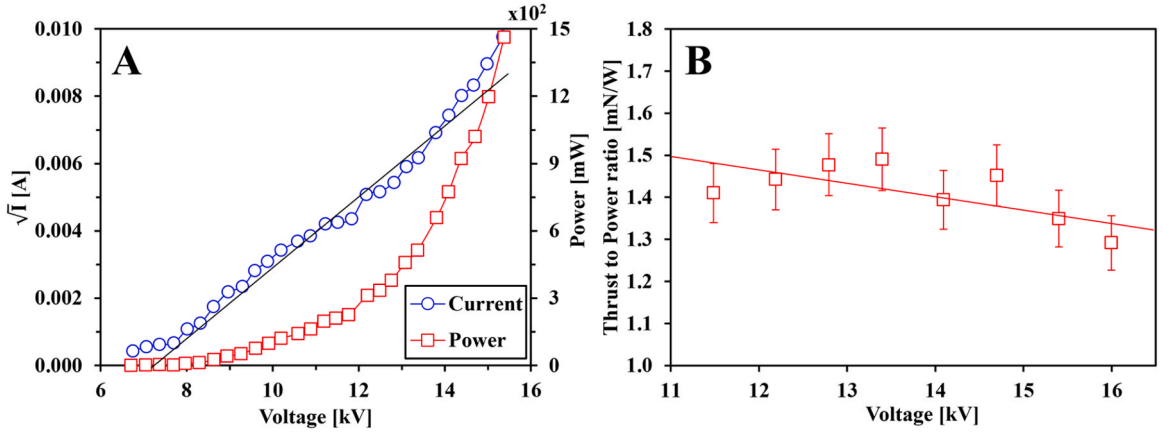

Fig. 7. Experimental results: **A)** Current-voltage & power-voltage characteristics of the discharge current by ion wind for the present wire-dielectric-water configuration; and **B)** Ratio of the thrust to power plotted vs the applied voltage using the flap's inclined angle $\delta = 45°$ and inter-electrode distance d = 15 mm.

example the positive corona with inter-electrode distance of 50 mm [44], the negative corona with inter-electrode distance of less than 15 mm for the configuration point-to-plane [43] and the point-to-plane based corona discharge. Recently, our research group has used this relationship to efficiently characterize bipolar corona discharge using asymmetric electrodes [28] and parallel pin geometry [45]. In addition, power consumption is also investigated with respect to the applied voltage. The relationship between power (P) and the applied voltage presented in Fig. 7A shows a maximum power consumption of about 1.5 W at applied voltage of 15 kV.

Furthermore, another imperative parameter to evaluate a propulsion system is the thrust-to-power ratio κ, which is considered as the ratio of the thrust (T) to power in this work as follows [35]

$$\kappa = \frac{T}{P}, \tag{10}$$

the efficiency of the present *i*Boat by the thrust-to-power ratio for a range of applied voltages from 11 kV to 16 kV as shown in Fig. 7B shows an average propulsion ratio of 1.45 mN/W. Compared to the thrust efficiency of existing EHD propulsion systems, i.e. 5 mN/W (wire-to-airfoil [35]), 5–15 mN/W (wire-to-cylinder [23,24,42]), the performance of our concept is in the same order but less competitive as not all of the lift is converted into thrust. Future modifications, such as flow-enhanced ducts [46] or additional high-voltage pulse [47], can be implemented to boost the performance of our wire-dielectric-water concept.

5. Conclusion

We demonstrated the first launch of an ion-wind powered miniaturized boat using a novel wire-dielectric-water configuration. Simulation results of our configuration elaborated the lift-to-thrust conversion mechanism, demonstrating the possibility of the new concept. Furthermore, experimental results consolidated the feasibility of utilizing the dielectric flap for adjusting ion flow, which allows to create a relevant thrust to propel *i*Boat within a range of applied voltages from 3 kV to 18 kV. A thrust-to-power ratio of 1.45 mN/W obtained by our simple wire-dielectric-water configuration demonstrates its capability yet implies the need for optimization. The obtained results have proven that the new concept yields promising applications of ion-wind powered boats for industry and military areas which require low noise and small power consumption.

CRediT authorship contribution statement

Dzung Viet Dao: Writing – review & editing, Project administration, Funding acquisition. **Van Thanh Dau:** Writing – review & editing, Project administration, Funding acquisition, Conceptualization. **Thien Xuan Dinh:** Software, Data curation. **Nam-Trung Nguyen:** Writing – review & editing, Project administration, Funding acquisition. **Canh-Dung Tran:** Writing – review & editing, Data curation. **Trung-Hieu Vu:** Data curation. **Tuan-Khoa Nguyen:** Writing – original draft, Investigation, Formal analysis, Data curation, Conceptualization. **Ngoc Luan Mai:** Writing – original draft, Software, Investigation, Formal analysis, Conceptualization.

Declaration of Competing Interest

The authors declare the following financial interests/personal relationships which may be considered as potential competing interests: Dzung Viet Dao reports financial support was provided by Australian Research Council. If there are other authors, they declare that they have no known competing financial interests or personal relationships that could have appeared to influence the work reported in this paper.

Acknowledgments

This work has been supported by Australian Research Council grant LP160101553 and was performed in part at the Queensland node of the Australian National Fabrication Facility (ANFF), a company established under the National Collaborative Research Infrastructure Strategy to provide nano and microfabrication facilities for Australian researchers. V.T. Dau thanks **Griffith University** for the research grant: “Bipolar electrostatic atomizing system - fundamental study and application”.

Appendix A. Supporting information

Supplementary data associated with this article can be found in the online version at doi:10.1016/j.sna.2024.116187.

Data availability

Data will be made available on request.

References

[1] A.P. Chattock, XLIV. On the velocity and mass of the ions in the electric wind in air, /11/01 1899, Lond. Edinb. Dublin Philos. Mag. J. Sci. 48 (294) (1899) 401–420, https://doi.org/10.1080/14786449908621431.
[2] M. Robinson, Movement of air in the electric wind of the corona discharge, Trans. Am. Inst. Electr. Eng. Part I: Commun. Electron. 80 (2) (1961) 143–150, https://doi.org/10.1109/TCE.1961.6373091.
[3] M. Goldman, A. Goldman, R.S. Sigmond, The corona discharge, its properties and specific uses 57 (9) (1985) 1353–1362, https://doi.org/10.1351/pac198557091353.
[4] D. Bessières, J. Paillol, N. Soulem, Negative corona triggering in air, /04/15 2004, J. Appl. Phys. 95 (8) (2004) 3943–3951, https://doi.org/10.1063/1.1667599.
[5] K. Yamada, An empirical formula for negative corona discharge current in point-grid electrode geometry, /09/01 2004, J. Appl. Phys. 96 (5) (2004) 2472–2475, https://doi.org/10.1063/1.1775301.
[6] A.M. Drews, L. Cademartiri, G.M. Whitesides, K.J.M. Bishop, Electric winds driven by time oscillating corona discharges, /10/14 2013, J. Appl. Phys. 114 (14) (2013) 143302, https://doi.org/10.1063/1.4824748.
[7] D.B. Go, S.V. Garimella, T.S. Fisher, R.K. Mongia, Ionic winds for locally enhanced cooling, /09/01 2007, J. Appl. Phys. 102 (5) (2007) 053302, https://doi.org/10.1063/1.2776164.
[8] C. Kim, D. Park, K.C. Noh, J. Hwang, Velocity and energy conversion efficiency characteristics of ionic wind generator in a multistage configuration, /02/01/ 2010, J. Electrost. 68 (1) (2010) 36–41, https://doi.org/10.1016/j.elstat.2009.09.001.
[9] E. Moreau, G. Touchard, Enhancing the mechanical efficiency of electric wind in corona discharges, /01/01/ 2008, J. Electrost. 66 (1) (2008) 39–44, https://doi.org/10.1016/j.elstat.2007.08.006.
[10] E. Bardy, M. Hamdi, M. Havet, O. Rouaud, Transient exergetic efficiency and moisture loss analysis of forced convection drying with and without electrohydrodynamic enhancement, /09/01/ 2015, Energy 89 (2015) 519–527, https://doi.org/10.1016/j.energy.2015.06.017.
[11] Z. Xia, R. Sun, F. Jing, S. Wang, H. Sun, G. Sun, Modeling and optimization of Scaffold-like macroporous electrodes for highly efficient direct methanol fuel cells, /07/01/ 2018, Appl. Energy 221 (2018) 239–248, https://doi.org/10.1016/j.apenergy.2018.03.100.
[12] Z. Wu, M. Bi, Z. Cao, S. Wang, X. Ye, Largely enhanced electrostatic generator based on a bipolar electret charged by patterned contact micro-discharge and optimized substrates, /05/01/ 2020, Nano Energy 71 (2020) 104602, https://doi.org/10.1016/j.nanoen.2020.104602.
[13] D.S. Drew, N.O. Lambert, C.B. Schindler, K.S.J. Pister, Toward controlled flight of the Ionocraft: a flying microrobot using electrohydrodynamic thrust with onboard sensing and no moving parts, IEEE Robot. Autom. Lett. 3 (4) (2018) 2807–2813, https://doi.org/10.1109/LRA.2018.2844461.
[14] M.J. Johnson, D.B. Go, Recent advances in electrohydrodynamic pumps operated by ionic winds: a review, /10/03 2017, Plasma Sources Sci. Technol. 26 (10) (2017) 103002, https://doi.org/10.1088/1361-6595/aa88e7.
[15] J. Zhang, L. Kong, J. Qu, S. Wang, Z. Qu, Numerical and experimental investigation on configuration optimization of the large-size ionic wind pump, /03/15/ 2019, Energy 171 (2019) 624–630, https://doi.org/10.1016/j.energy.2019.01.086.
[16] S. Nangle-Smith, J.S. Cotton, EHD-based load controllers for R134a convective boiling heat exchangers, /12/01/ 2014, Appl. Energy 134 (2014) 125–132, https://doi.org/10.1016/j.apenergy.2014.07.061.
[17] A. Rashkovan, E. Sher, H. Kalman, Experimental optimization of an electric blower by corona wind, /10/01/ 2002, Appl. Therm. Eng. 22 (14) (2002) 1587–1599, https://doi.org/10.1016/S1359-4311(02)00082-0.
[18] I.Y. Chen, M.-Z. Guo, K.-S. Yang, C.-C. Wang, Enhanced cooling for LED lighting using ionic wind, /01/15/ 2013, Int. J. Heat. Mass Transf. 57 (1) (2013) 285–291, https://doi.org/10.1016/j.ijheatmasstransfer.2012.10.015.

[19] P.J. McKinney, J.H. Davidson, D.M. Leone, Current distributions for barbed plate-to-plane coronas, IEEE Trans. Ind. Appl. 28 (6) (1992) 1424–1431, https://doi.org/10.1109/28.175297.
[20] C. Zhai, et al., An electrostatic discharge based needle-to-needle booster for dramatic performance enhancement of triboelectric nanogenerators, /12/01/ 2018, Appl. Energy 231 (2018) 1346–1353, https://doi.org/10.1016/j.apenergy.2018.09.120.
[21] P. Zhao, S. Portugal, S. Roy, Efficient needle plasma actuators for flow control and surface cooling, /07/20 2015, Appl. Phys. Lett. 107 (3) (2015) 033501, https://doi.org/10.1063/1.4927051.
[22] B. Kim, S. Lee, Y.S. Lee, K.H. Kang, Ion wind generation and the application to cooling, /10/01/ 2012, J. Electrost. 70 (5) (2012) 438–444, https://doi.org/10.1016/j.elstat.2012.06.002.
[23] E. Moreau, N. Benard, J.-D. Lan-Sun-Luk, J.-P. Chabriat, Electrohydrodynamic force produced by a wire-to-cylinder dc corona discharge in air at atmospheric pressure, /10/28 2013, J. Phys. D: Appl. Phys. 46 (47) (2013) 475204, https://doi.org/10.1088/0022-3727/46/47/475204.
[24] C.K. Gilmore, S.R.H. Barrett, Electrohydrodynamic thrust density using positive corona-induced ionic winds for in-atmosphere propulsion, /03/08 2015, Proc. R. Soc. A Math. Phys. Eng. Sci. 471 (2175) (2015) 20140912, https://doi.org/10.1098/rspa.2014.0912.
[25] J. Darabi, C. Rhodes, CFD modeling of an ion-drag micropump, 02/01, Sens. Actuators A: Phys. 127 (2006) 94–103, https://doi.org/10.1016/j.sna.2005.10.051.
[26] Z. Li, Y. Liu, Y. Xing, T.-M.-P. Tran, T.-C. Le, C.-J. Tsai, Novel wire-on-plate electrostatic precipitator (WOP-EP) for controlling fine particle and nanoparticle pollution, /07/21 2015, Environ. Sci. Technol. 49 (14) (2015) 8683–8690, https://doi.org/10.1021/acs.est.5b01844.
[27] V.T. Dau, T.X. Dinh, T.T. Bui, T. Terebessy, Corona anemometry using dual pin probe, /04/15/ 2017, Sens. Actuators A: Phys. 257 (2017) 185–193, https://doi.org/10.1016/j.sna.2017.02.025.
[28] V.T. Dau, T.X. Dinh, T. Terebessy, T.T. Bui, Ion wind generator utilizing bipolar discharge in parallel pin geometry, IEEE Trans. Plasma Sci. 44 (12) (2016) 2979–2987, https://doi.org/10.1109/TPS.2016.2580574.
[29] V.T. Dau, T.T. Bui, T.X. Dinh, T. Terebessy, Pressure sensor based on bipolar discharge corona configuration, /01/01/ 2016, Sens. Actuators A Phys. 237 (2016) 81–90, https://doi.org/10.1016/j.sna.2015.11.024.
[30] E.A. Christenson, P.S. Moller, Ion-neutral propulsion in atmospheric media, /10/01 1967, AIAA J. 5 (10) (1967) 1768–1773, https://doi.org/10.2514/3.4302.
[31] H.D.P.Jack Wilson, William K. Thompson, An Investigation of Ionic Wind Propulsion, NASA/TM-2009-215822, 2009.
[32] L. Pekker, M. Young, A model of an ideal electrohydrodynamic thruster, 08/04, J. Propuls. Power 27 (2010) 17, https://doi.org/10.2514/1.B34097.
[33] C. Kim, K.-C. Noh, S.-Y. Kim, J. Hwang, Electric propulsion using an alternating positive/negative corona discharge configuration composed of wire emitters and wire collector arrays in air, /09/12 2011, Appl. Phys. Lett. 99 (11) (2011) 111503, https://doi.org/10.1063/1.3636409.
[34] M. Chirita, A. Ieta, Toroidal counter electrode for ionic propulsion, /11/08 2022, Sci. Rep. 12 (1) (2022) 19002, https://doi.org/10.1038/s41598-022-23377-5.
[35] H. Xu, et al., Flight of an aeroplane with solid-state propulsion, /11/01 2018, Nature 563 (7732) (2018) 532–535, https://doi.org/10.1038/s41586-018-0707-9.
[36] V.Y. Khomich, I.E. Rebrov, In-atmosphere electrohydrodynamic propulsion aircraft with wireless supply onboard, /10/01/ 2018, J. Electrost. 95 (2018) 1–12, https://doi.org/10.1016/j.elstat.2018.07.005.
[37] J.S. Chang, P.A. Lawless, T. Yamamoto, Corona discharge processes, IEEE Trans. Plasma Sci. 19 (6) (1991) 1152–1166, https://doi.org/10.1109/27.125038.
[38] L. Zhao, K. Adamiak, EHD flow in air produced by electric corona discharge in pin–plate configuration, /03/01/ 2005, J. Electrost. 63 (3) (2005) 337–350, https://doi.org/10.1016/j.elstat.2004.06.003.
[39] K. Adamiak, P. Atten, Simulation of corona discharge in point–plane configuration, /06/01/ 2004, J. Electrost. 61 (2) (2004) 85–98, https://doi.org/10.1016/j.elstat.2004.01.021.
[40] L. Zhao, K. Adamiak, EHD gas flow in electrostatic levitation unit, /07/01/ 2006, J. Electrost. 64 (7) (2006) 639–645, https://doi.org/10.1016/j.elstat.2005.10.017.
[41] H. Toyota, S. Zama, Y. Akamine, S. Matsuoka, K. Hidaka, Gaseous electrical discharge characteristics in air and nitrogen at cryogenic temperature, IEEE Trans. Dielectr. Electr. Insul. 9 (6) (2002) 891–898, https://doi.org/10.1109/TDEI.2002.1115482.
[42] K. Masuyama, S.R.H. Barrett, On the performance of electrohydrodynamic propulsion, /06/08 2013, Proc. R. Soc. A: Math., Phys. Eng. Sci. 469 (2154) (2013) 20120623, https://doi.org/10.1098/rspa.2012.0623.
[43] X. Meng, H. Zhang, J. Zhu, A general empirical formula of current–voltage characteristics for point-to-plane geometry corona discharges, /02/29 2008, J. Phys. D: Appl. Phys. 41 (6) (2008) 065209, https://doi.org/10.1088/0022-3727/41/6/065209.
[44] G.F.L. Ferreira, O.N. Oliveira, J.A. Giacometti, Point-to-plane corona: current-voltage characteristics for positive and negative polarity with evidence of an electronic component, /05/01 1986, J. Appl. Phys. 59 (9) (1986) 3045–3049, https://doi.org/10.1063/1.336926.
[45] V.T. Dau, C.D. Tran, T.X. Dinh, L.B. Dang, T. Terebessy, T.T. Bui, Estimating the effect of asymmetric electrodes in bipolar discharge ion wind generator, IEEE Trans. Dielectr. Electr. Insul. 25 (3) (2018) 900–907, https://doi.org/10.1109/TDEI.2018.006881.
[46] C.L. Nelson, D.S. Drew, High aspect ratio multi-stage ducted electroaerodynamic thrusters for micro air vehicle propulsion, IEEE Robot. Autom. Lett. 9 (3) (2024) 2702–2709, https://doi.org/10.1109/LRA.2024.3355728.
[47] E. Moreau, P. Audier, T. Orriere, N. Benard, Electrohydrodynamic gas flow in a positive corona discharge, J. Appl. Phys. 125 (13) (2019) 133303, https://doi.org/10.1063/1.5056240.

Ngoc Luan Mai received the B. Eng. and M. Eng. degrees in Aerospace Engineering from Ho Chi Minh City University of Technology, in 2019 and 2023, respectively. He is awarded the Griffith University Postgraduate Research Scholarships (GUPRS) and Griffith University International Postgraduate Research Scholarships (GUIPRS) and currently a Ph.D. candidate at Griffith University, Australia. His research interests are developing both experiments and simulations relevant to microfluidics, electro-hydrodynamics, MEMS.

Tuan-Khoa Nguyen is a Griffith University Postdoctoral Fellow (GUPF). He received his Ph.D. in 2018 at the Queensland Micro- and Nanotechnology Centre (QMNC), Griffith University. His research involves electronics and material developments of solid state and wide band gap materials for miniaturized physical sensing and bio-electronic applications. He has authored and co-authored over 60 high impact factor journal papers. Dr. Nguyen research focuses on the innovation and development of micro, nano-scaled electronics devices for emerging aspects in sensing, and biological applications.

Canh Dung Tran is an associate professor in Mechanical and Mechatronic Engineering at the University of Southern Queensland. He has authored and co-authored over 100 high impact factor scientific articles. His research interests include

Trung-Hieu Vu received the B.S degree in Mechanical Engineering from Griffith University, Australia in 2020. He is currently working on his PhD at Griffith in fabrication of nanoparticles and nanofibers via electrospray/electrospinning. Electrohydrodynamics and microfluidics are his main research subjects.

Thien Xuan Dinh received the B. S. degree in Aerospace Engineering from Ho Chi Minh City University of Technology in 2002, Vietnam and the M. Sc. and Ph.D. degrees in mechanical engineering from Ritsumeikan University in 2004 and 2007, respectively. He was recipient of Japan Government Scholarship (MEXT) for Outstanding Student to pursuits his M. Sc. and Ph. D. courses and Japan Society for the Promotion of Science postdoctoral fellowship from 2011 to 2013. His general research interest is computation of fluid flow. The large parts of his research are turbulence modelling using Large Eddy Simulation, multiphase modelling using Volume of Fluid technique, and simulation of turbulence and dispersion. Currently, at CSIRO, his work focuses on the CFD modelling for the mineral processes. His research interest are metallurgy flows, supersonic quenching processes, population balance in solid/liquid multiphase flows, and mixing flows.

Nam-Trung Nguyen Nam-Trung Nguyen received his Dipl-Ing, Dr Ing, and Dr Ing Habil degrees from Chemnitz University of Technology, Germany, in 1993, 1997, and 2004, respectively. He is a Fellow of ASME and a Senior Member of IEEE. His research is focused on microfluidics, nanofluidics, micro/ nanomachining technologies, micro/nanoscale science, and instrumentation for biomedical applications.

Dzung Viet Dao received his Ph.D. degree from Ritsumeikan University, Japan in 2003. He then served as a Postdoctoral Research Fellow from 2003 to 2006, a Lecturer from 2006 to 2007, and a Chair Professor from 2007 to 2011, all at Ritsumeikan University. From 2011 A/Prof Dao joined Griffith University, Australia, where he has been teaching in Mechatronics and Mechanical Engineering. His current research interests include advanced manufacturing, MEMS sensors & actuators, transducers for harsh environments, and mechatronics/robotics.

Van Thanh Dau received the B.S. degree in aerospace engineering from Hochiminh City University of Technology, Vietnam, in 2002, and the M.S. and Ph.D. degrees in micromechatronics from Ritsumeikan University, Japan, in 2004 and 2007, respectively. From 2007–2009, he was a Postdoctoral Fellow with Japan Society for the Promotion of Science (JSPS) at Micro Nano Integrated Devices Laboratory, Ritsumeikan University. Since 2010 he has been with Research Group, Sumitomo Chemical Co. Ltd., where he works on integrated micro electrospray and atomization methods. He is currently a Senior Lecturer at School of Engineering and Built Environment, Griffith University, Australia. His current research subjects are micro fluidics, electro hydrodynamics, microsensors and microactuators. He is the author and co-author of more than 70 scientific articles and 17 inventions.